Crashworthiness analysis of structures made from polymers

P.A. Du Bois[1], M. Koesters[2], T. Frank[2] & S. Kolling[2]

[1]*Consulting Engineer, Freiligrathstr. 6, 63071 Offenbach, Germany*
[2] *Northeastern University, Departement of Structural Engineering, Boston, MA 02115, USA*
[3] *DaimlerChrysler AG, EP/CSB, HPC X411, 71059 Sindelfingen*

Abstract:

A comparative review of material models for polymers subjected to impact loading is presented. Due to the different material models, polymers are classified in incompressible elastomers, compressible foams and thermoplastics. Elastomers and recoverable foams are based on the same theoretical description: hyperelasticity. We present a material law which allows fast generating of input data based on uniaxial static and dynamic tensile tests at different strain rates. As an application, the deformation behavior of a Hardy disk during a frontal offset impact is investigated. For thermoplastics, we give an overview of suitable material laws and show how the behavior can be characterized approximately by using metal plasticity. On the basis of a three-point bending test, the predictions of the presented approaches are compared critically. Some typical applications of polymer modeling in modern crash simulation are shown by means of pedestrian protection.

Keywords: Explicit Finite Elements, Short-time Dynamics, Crash Simulation, Pedestrian Protection, Material Modeling, Thermoplastics, Foams, Elastomers

Abbreviations: EMI - Ernst Mach Institute, Freiburg, Germany
FAT – German Association for Automotive Research

1 Introduction

The numerical simulation of structural parts made from polymers is becoming increasingly important. Although highly sophisticated material laws are available in commercial finite element programs, there are still open questions, especially for crashworthiness analysis. In this paper, we restrict our attention to the explicit solver of LS-DYNA, see [1] and [2]. However, the results are transferable to other solvers without qualification. We present an overview of both classical and new material models for polymers which are used for crash simulations. For this purpose, it is useful to classify polymers in elastomers, foams and thermoplastics.
For quasi-static problems, elastomers can be considered as incompressible rubber-like materials. For this class of materials, a large number of models are available in LS-DYNA, e.g. the material laws by Blatz and Ko [3], Mooney and Rivlin [4], [5] and Ogden [6]. In short-time dynamics, however, a strong strain rate dependency of elastomers can be observed. For crash simulations, if the strain rate varies in dependence on the location, this material behavior has also to be taken into account. To consider this behavior, the Ogden material has been generalized by viscous terms. A disadvantage of such a material description is the large number of parameters which has to be identified for each material. Usually, the parameter identification is quiet complex and time consuming. Therefore, we developed a

new material model, see [7], based on the Ogden formulation and implemented it into LS-DYNA. In this model, stress-strain curves received from uniaxial static and dynamic tensile tests can directly be entered and no parameter identification is necessary anymore. Important applications of rubber-like materials are given by the modeling of the PVB-interlayer of a windscreen consisting of laminated glass [8], and the Hardy-disk [9].
For the second class of polymeric materials, foams, the same theoretical background as for elastomers can be used: hyperelasticity. In LS-DYNA, a material law for foams is available which is based, again, on tabulated stress strain curves directly obtained by experimental tests.
For the third class of polymeric materials, thermoplastics, we have non-linear elasticity and, in addition, a plastic behavior of the material. Since thermoplastics are not incompressible during plastic flow the commonly used material laws based on von Mises plasticity are not suitable. Taking a three point bending test as an example, we demonstrate the use of a Drucker-Prager model that takes the compressibility and the different behavior of the material under tensile and compressive stress into account. Important applications of polymeric materials in automotive structures are associated with pedestrian protection, e.g. head and leg impact, see [10], [16] and [17].

2 Material Formulations

In industrial environment, only limited time is available to produce simulation results. The most efficient material laws from a user point of view are undoubtedly based on tabulated stress-strain curves obtained directly from physical testing. That way, although some smoothing of the raw test data may be required for reasons of numerical stability, time-consuming fitting operations needed for analytical formulations can be entirely avoided. It should be emphasized, however, that predictable analysis is necessarily based on experimental material testing. In what follows, we briefly review the main classes of material formulations as they are implemented in the LS-DYNA package.

2.1 Hyperelasticity

The most straight forward generalization of Hooke's law to large displacements and large deformations is hyperelasticity, see [14], [15]. A hyperelastic material is path independent and allows to calculate the second Piola-Kirchhoff stress tensor $\mathbf{S} = 2\partial W / \partial \mathbf{C}$ from a derivative of the energy functional $W = \hat{W}(\mathbf{C})$ with respect to the components of the right Cauchy-Green strain tensor $\mathbf{C} = \mathbf{F}^T\mathbf{F}$, where $\mathbf{F} = \mathrm{Grad}\,\mathbf{x}$ is the deformation gradient. In LS-DYNA we can distinguish two families of hyperelastic materials. The first one is based on an energy functional expressed in the invariants of the right Cauchy-Green tensor: $W = \hat{W}(I_C, II_C, III_C)$. The invariants of $\mathbf{C}$ are given by $I_C = \mathbf{1} : \mathbf{C} = \mathrm{tr}\,\mathbf{C}$, $II_C = \frac{1}{2}\left(I_C^2 - \mathbf{C} : \mathbf{C}\right)$ and $III_C = \det \mathbf{C}$. Then, the derivative yields

$$\mathbf{S} = 2\frac{\partial W}{\partial I_C}\mathbf{1} + 2\frac{\partial W}{\partial II_C}\left(I_C\mathbf{1} - \mathbf{C}\right) + 2\frac{\partial W}{\partial III_C}III_C\mathbf{C}^{-1}. \qquad (1)$$

The Cauchy stress $\boldsymbol{\sigma}$ can now be obtained by forming $\boldsymbol{\sigma} = J^{-1}\mathbf{F}\mathbf{S}\mathbf{F}^T$, where $J = \det \mathbf{F}$ is the relative volume.
The second family of hyperelastic materials is formulated in terms of principle stretch ratios. Therefore, it is instructive to rewrite the former expressions in terms of principal stretches λ_i. After a decomposition $\mathbf{F} = \mathbf{R}\mathbf{U}$, where $\mathbf{R}^T\mathbf{R} = \mathbf{1}$ and $\mathbf{U} = \mathbf{U}^T$, the invariants are given by $I_C = \lambda_1^2 + \lambda_2^2 + \lambda_3^2$, $II_C = \lambda_1^2\lambda_2^2 + \lambda_2^2\lambda_3^2 + \lambda_3^2\lambda_1^2$, $III_C = \lambda_1^2\lambda_2^2\lambda_3^2 = J^2$ and the Cauchy stress $\boldsymbol{\sigma}$ and the principal engineering stress $\boldsymbol{\tau}$ can be obtained as

$$\sigma_i = \frac{1}{\lambda_j\lambda_k}\frac{\partial W}{\partial \lambda_i} \Rightarrow \lambda_j\lambda_k\sigma_i =: \tau_i = \frac{\partial W}{\partial \lambda_i}. \qquad (2)$$

The Blatz-Ko [3] implementation in LS-DYNA corresponds to the following energy function:

$$W = \frac{\mu}{2}\left(I_C + \frac{1}{\alpha}\left(III_C^{-2\alpha} - 1\right) - 3\right). \qquad (3)$$

The parameter $\alpha = \nu/(1-2\nu)$ is related to Poisson's ratio ν.
A standard function to describe hyperelastic behavior is the material law given by Mooney and Rivlin, see [4] and [5]:

$$W(I_C, II_C, III_C) = A\left(I_C - 3\right) + B\left(II_C - 3\right) + C\left(\frac{1}{III_C^2} - 1\right) + D\left(III_C - 1\right)^2. \quad (4)$$

Here, *A* and *B* are material parameters. The last two expressions with the parameters *C* and *D* are hydrostatic terms:

$$C = \frac{A}{2} + B \quad \text{and} \quad D = \frac{A\left(5\nu - 2\right) + B\left(11\nu - 5\right)}{\left(2 - 4\nu\right)}. \quad (5)$$

As an example of a hyperelastic laws formulated in terms of principle stretches we mention the Ogden law:

$$W = \sum_{i=1}^{3}\sum_{j=1}^{n}\frac{\mu_j}{\alpha_j}\left(\lambda_i^{*\alpha_j} - 1\right) + K(J - 1 - \ln J) \Rightarrow \sigma_i = \sum_{p=1}^{n}\frac{\mu_p}{J}\left[\lambda_i^{*\alpha_p} - \sum_{k=1}^{3}\frac{\lambda_k^{*\alpha_p}}{3}\right] + K\frac{J-1}{J}. \quad (6)$$

Here, α_j are non-integer, $J = \lambda_1\lambda_2\lambda_3$ and $\lambda_i^* = \lambda_i J^{-1/3}$. Note that the penalty term corresponds to a purely hydrostatic stress and, therefore, the deviatoric part of the Ogden functional generates a zero stress in the undeformed configuration. In LS-DYNA, a tabulated version of the Ogden material law has been implemented with the material law "MAT_SIMPLIFIED_RUBBER". Here, the Ogden functional (7) is internally determined from the uniaxial engineering stress-strain curve by defining a tabulated function of the principal stretch ratio as follows [7]:

$$f(\lambda) = \sum_{p=1}^{n}\mu_p\lambda^{*\alpha_p} \quad \Rightarrow \quad \sigma_i = \frac{1}{J}\left(f(\lambda_i) - \frac{1}{3}\sum_{j=1}^{3}f(\lambda_j)\right) + K\frac{J-1}{J}. \quad (7)$$

An overview of further hyperelastic laws which are implemented in LS-DYNA is given in Table 1.

Law	Keyword
7	MAT_BLATZ-KO_RUBBER
2	MAT_ORTHOTROPIC_ELASTIC
33	MAT_FRAZER-NASH_RUBBER
27	MAT_MOONEY-RIVLIN_RUBBER
38	MAT_BLATZ-KO_FOAM
83	MAT_FU_CHANG_FOAM
181	MAT_SIMPLIFIED_RUBBER

Table 1: Overview of hyperelastic materials in LS-DYNA.

2.2 Viscosity

Viscoelastic material laws in LS-DYNA are based on hypoelasticity. In such a hypoelastic formulation, the objective stress rate is derived directly from the strain rate or rate of deformation tensor. In the particular case of LS-DYNA, stress rates according to Jaumann are chosen. It is well known, that the use of the Jaumann rate leads to an oscillatory response under large shear deformations. The difference between hyper- and hypoelasticity in the case of simple shear is illustrated in Figure 1b, curve A (hypoelastic) and C (hyperelastic, Blatz-Ko). It can be clearly seen from the picture that the differences are negligible for small shear strains. It should be emphasized that problems with hypoelastic material laws only occur for large deformations and not for large rotations. Therefore, hypoelastic formulations are adequate for the description of large rotation / small deformation problems.
Hypoelasticity is easily generalized to include time-dependency of the stress. However, in this case the reversibility of the material law is lost.

a) Material 7 (A) and 77 (B,C,D) b) Material 1(A), 6(B), 7(C) and 76(D)

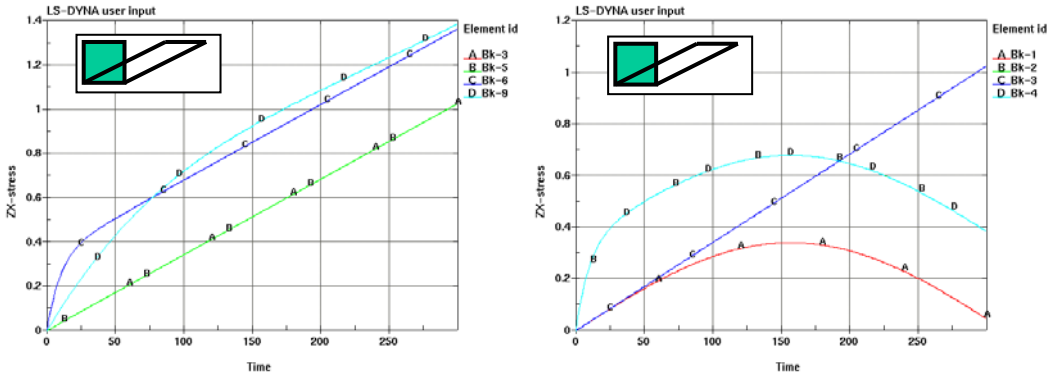

Figure 1: Simple shear behavior for hypo- and hyperelastic materials

This allows considering phenomena such as hysteresis, rate dependency, stress relaxation and creep. In linear hereditary material laws or Boltzmann laws, deviatoric stresses s and hydrostatic stresses p are computed by a convolution integral of the strain rate and the relaxation function:

$$\mathrm{s} = \int_0^t 2g(t-\tau)\dot{\varepsilon}_{\mathrm{d}}(\tau)d\tau, \quad p = \int_0^t k(t-\tau)\dot{\varepsilon}_v(\tau)d\tau \tag{8}$$

The relaxation function is nothing else than a time-dependent modulus, i.e. if the function is constant in time, hypoelasticity is recovered: $\mathrm{g} = \mu$ and $k = K$. The resulting stresses are linear in the strain rate which is typical for high Polymers at small strain. Note that linear viscoelasticity is often based on a Prony (exponential) series where up to six exponential terms are used in the relaxation function. A selection of viscoelastic laws which are available in LS-DYNA are listed in Table 2.

Law	Keyword
6	MAT_VISCOELASTIC
60	MAT_ELASTIC_WITH_VISCOSITY
61	MAT_KELVIN-MAXWELL_VISCOELASTIC
62	MAT_VISCOUS_FOAM
76	MAT_GENERAL_VISCOELASTIC

Table 2: Overview of viscoelastic materials in LS-DYNA.

In Figure 1, some simple shear test simulation results are presented. A linear response is obtained for the quasistatic case where hyperelastic material laws are used, compare curves A and B in Figure 1a and curve C in Figure 1b. Hypoelastic material laws show the well known Jaumann rate type of response (curve A in Figure 1b). In the dynamic case, LS-DYNA uses a Jaumann formulation to evaluate the viscous stress terms as can be seen in curves B and D in Figure 1b. Depending on the used relaxation times, the Jaumann-type effects will be more or less pronounced, see curves C and D in Figure 1a.

Law	Keyword
57	MAT_LOW_DENSITY_FOAM
73	MAT_LOW_DENSITY_VISCOUS_FOAM
77	MAT_HYPERELASTIC_RUBBER
87	MAT_CELLULAR_RUBBER
127	MAT_ARRUDA_BOYCE

Table 3: Overview of coupled hyperelastic- viscoelastic materials in LS-DYNA.

For the description of the behavior of polymeric materials, a combination of hyperelastic and viscoelastic law often is required. Such material models are also available in LS-DYNA. In addition to the tables before, we list a selection of combined hyperelastic-viscoelastic material laws in Table 3.

2.3 Plasticity

Elastic-plastic material laws have been developed historically for the description of metallic materials based on crystal plasticity. The most commonly used example of this type implemented in LS-DYNA is MAT_PIECEWISE_LINEAR_PLASTICITY. The same approach can be applied to some degree to the simulation of thermoplastics. However, it should be noted that very important differences exist between metals and thermoplastics. In particular, plastics have no constant modulus of elasticity and the different yield criterions under tension and compression preclude the use of a von Mises type of yield surface. Furthermore, the hardening of thermoplastics is anisotropic and the plastic deformation does not happen at constant volume. This lack of plastic incompressibility requires a flow rule allowing for permanent volumetric deformation. None of these effects can be considered in a classical metallic elastic-plastic material law. For an overview, some materials considering plasticity limited to materials with isotropic behavior are listed in Table 4.

Law	**Keyword**	Hardening	Rate effect
3	MAT_PLASTIC_KINEMATIC	Linear	CS
12	MAT_ISOTROPIC_ELASTIC_PLASTIC	Linear	CS
15	MAT_JOHNSON_COOK	Power law	JC
18	MAT_POWER_LAW_PLASTICITY	Power law	CS
19	MAT_STRAIN_RATE_DEPENDENT_PLASTICITY	Linear	load curves
24	MAT_PIECEWISE_LINEAR_PLASTICITY	Load curve	CS, tabulated
81	MAT_PLASTICITY_WITH_DAMAGE	Load curve	CS, tabulated
89	MAT_PLASTICITY_POLYMER	Load curve	CS, tabulated
98	MAT_SIMPLIFIED_JOHNSON_COOK	Power law	JC
105	MAT_DAMAGE_2 (VISCO-PLASTIC)	Power law	Perzyna
112	MAT_FINITE_ELASTIC_STRAIN_PLASTICITY	Load curve	CS, tabulated
123	MAT_MODIFIED_PIECEWISE_LINEAR_PLASTICITY	Load curve	Load curve

Table 4: Overview of plastic materials in LS-DYNA.

3 Elastomers (rubber-like materials)

The usage of elastomers for safety relevant parts in automotive structures and, therefore, their consideration in crash simulation is getting increasingly important. Without claiming completeness, we mention adhesives (windscreen/structural parts), rubber doughnuts (Hardy disk), rubber supports (bushings, gaskets) and head impactor skins used for pedestrian protection tests.
If we consider elastomers to be nearly incompressible we may use hyperelastic laws and coupled hyperelastic-viscoelastic laws respectively. As a straight forward approach to model elastomers, we recommend the use of the aforementioned MAT_SIMPLIFIED_RUBBER to avoid time consuming parameter identification.
It is interesting to note that a purely hyperelastic law without consideration of rate-dependency can give sufficient accuracy for many applications provided that the large shear deformations in the rubber parts that occur during a crash event can be accommodated by the mesh. An example hereof is shown in the simulation of a Hardy disk during a frontal impact, see Figure 2.
The simulation of directly impacted rubber parts such as the skins of head impactor devices for pedestrian protection testing is more complicated since the rate effects tend to be the dominating part in the material response.

4 Foams

The numerical simulation of low density foams has been the subject of an intensive research program by a FAT program between 1996 and 2003. Four different foams with density around 50g/l (RG 50)

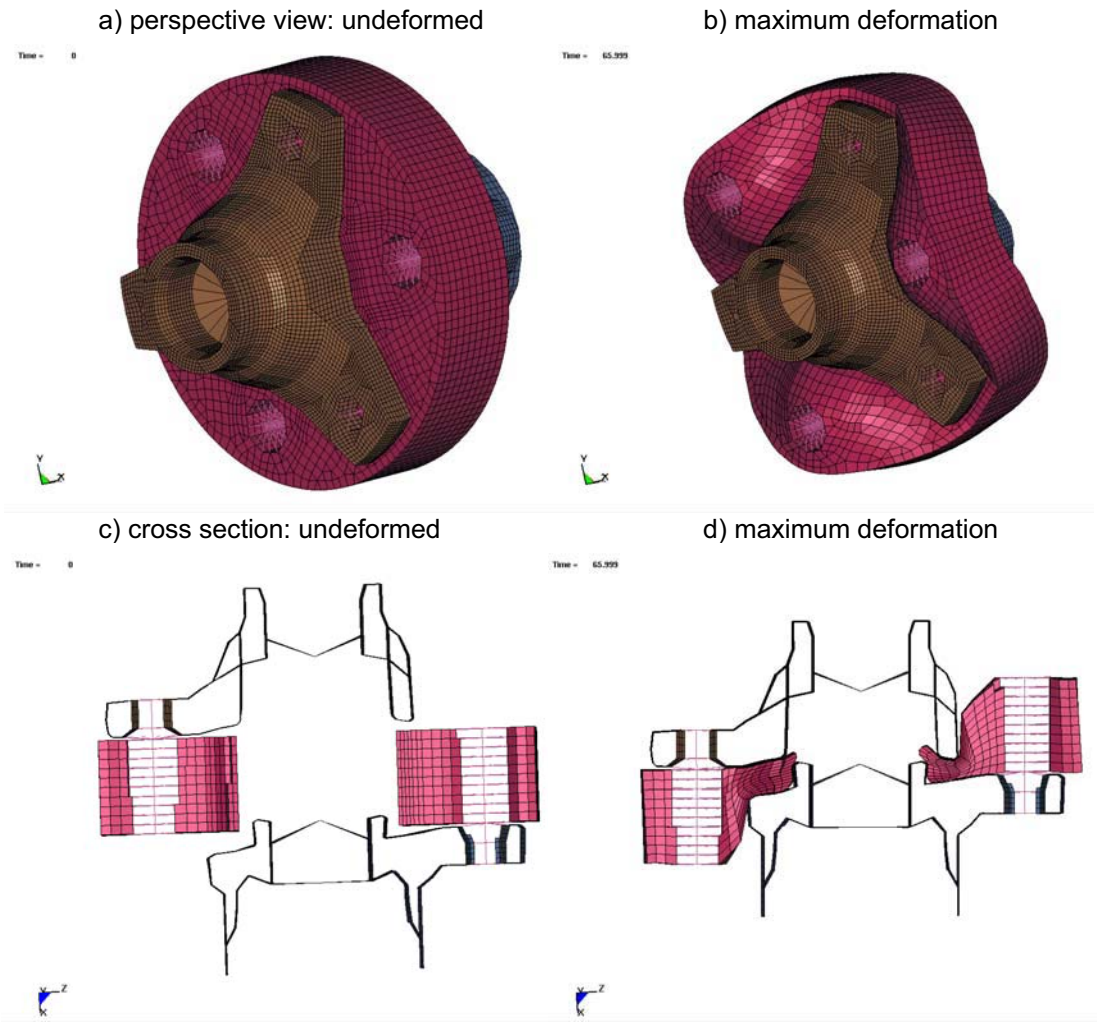

Figure 2: Hardy-disk during frontal offset impact

were selected: seat foam, a padding foam and two different bumper foams on the basis of polyurethane (PU) and polypropylene (PP).
Around 300 tests were performed for each foam by EMI, these involved basic quasi static and dynamic material testing as well as validation tests under dynamic loading. The validation tests included drop-tests performed with spherical impactors under different angles and velocities. In the case of LS-DYNA, the FAT program allowed to define methodologies for the industrial simulation of each of the four foam classes using essentially MAT_FU-CHANG_FOAM and MAT_VISCOUS_FOAM to represent elastic foams and MAT_CRUSHABLE_FOAM and/or MAT_BILKHU-DUBOIS_FOAM for the representation of foams featuring permanent deformations. Criteria in terms of accuracy, efficiency (timestep) and stability were met partly by improvements in the software as well as by proper definition of input data.
A smooth definition of the curves turned out to be essential mainly for numerical stability. Some results of a drop-test for a polyurethane bumper foam are shown if Figure 3. The extremely high compressibility of these foams is easily noticed. A stable numerical simulation of these high deformations is necessary to perform accurate simulation of automotive components, e.g. bumper tests and leg impact for pedestrian protection.
To sum up, it can be said that for the simulation of standard low density foams, a satisfactory state-of-the-art has been achieved. Some problems though remain. In particular the simulation of higher density foams remains largely uninvestigated. Some phenomena such as brittle rupture and lateral bulging are an issue with this class of materials. In the case of soft polyurethane, e.g. seat foams, a dependency of the material characteristics upon size and shape of the specimen was observed. This effect can currently not be simulated; approaches involving the theory of porous media represent a possibility for the future. Finally, high deformation gradients can occur if sharp objects penetrate the foam component. This will generally lead to element inversion as long as the finite element mesh consists of

Lagrangean solid elements. The use of alternative discretization techniques, e.g. mesh-free Galerkin, should be investigated to avoid negative volumes.

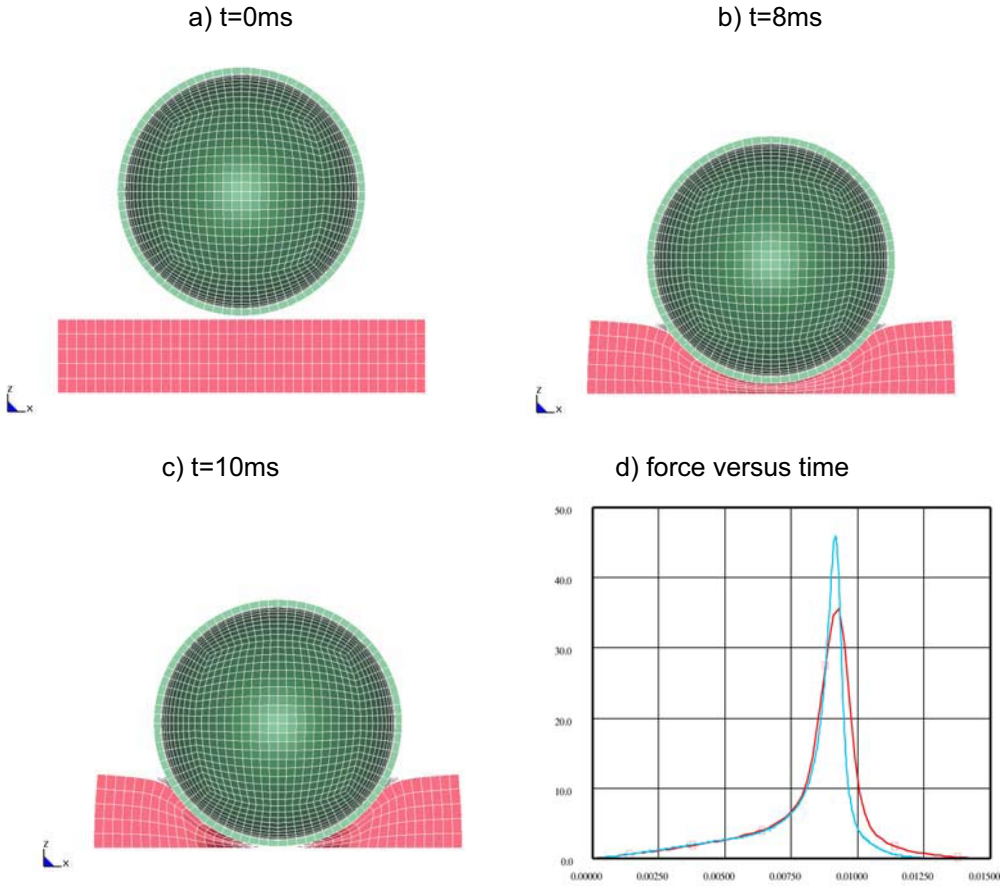

Figure 3: Validation test for foam models

In general, it should be noticed that due to global and local density variations as well as skin formation in cold formed parts, the response of foam components can diverse considerably. This by itself limits the degree of accuracy that can be achieved with numerical methods. The influence of climate conditions (temperature and humidity) on the response of foam materials may further complicate the situation.

5 Thermoplastics

Under high velocity impact loading, thermoplastic components undergo large plastic deformations and will most likely fail. Consequently, the unloading behavior is irrelevant and thermoplastics can be modeled with a pretty good approximation as pseudo-metallic elastic-plastic bodies. This is, however, not always the case. An important application in crash simulation for a more accurate modeling of thermoplastics is the behavior of a bumper fascia during leg impact in pedestrian protection. Here, it is essential to compute the internal energy of the bumper fascia to determine the correct bending angle of the leg as a measure of loading due to the impact. The problem is that in this loading case the bumper fascia will typically undergo only small straining and the deflection will be largely elastic. The unloading phase is of fundamental importance for the determination of the bending angle in the leg-form.
The viscoelastic response of the thermoplastic under the yield surface must, consequently, be modeled and this is not the case in traditional elastic-plastic material laws which consider the material response to be linear elastic up until yield. In Figure 4, stress-strain curves are depicted for a typical bumper fascia material, a thermoplastic elastomeric olefin resin. The strain rate behavior is similar to what is known for steels. However, not only an increasing plastic behavior is detectable if we increase the strain rate; an increasing modulus of elasticity can be measured too. Moreover, a distinct nonlinear elastic part can be observed but cannot be modeled by a purely linear elastic-plastic law.

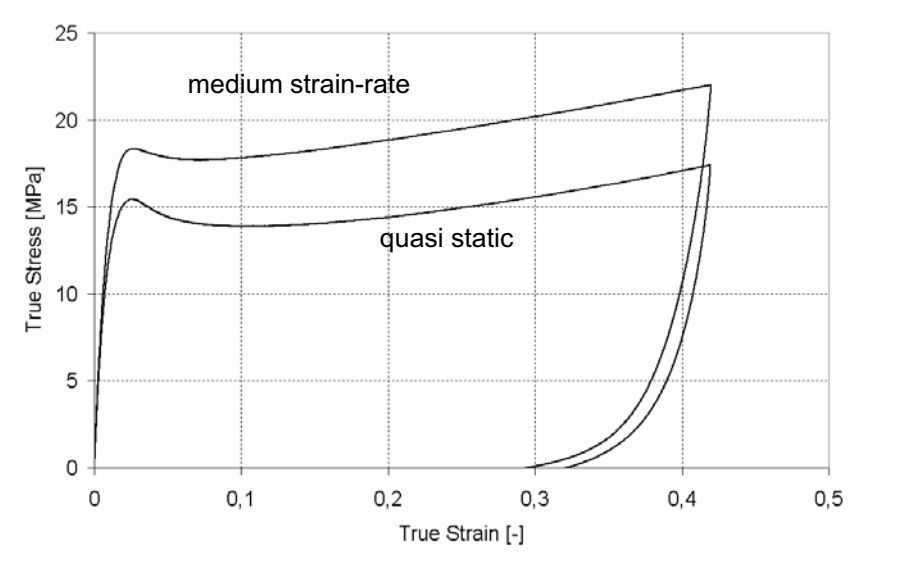

Figure 4: Stress-Strain curves for PP-EPDM

The true stress-true strain curve in *Figure 4* shows a reversal of curvature indicating a softening phase that is followed by a hardening phase. For the deformation of the dog-bone specimen, this means that necking will occur at very low strains corresponding to the initial softening of the material. The subsequent hardening, however, results in a stabilization of the necked area and a redistribution of the plastic strains over the entire specimen. Unlike metals, the primary energy-absorbing potential of the thermoplastic resides at plastic strains beyond the necking value.

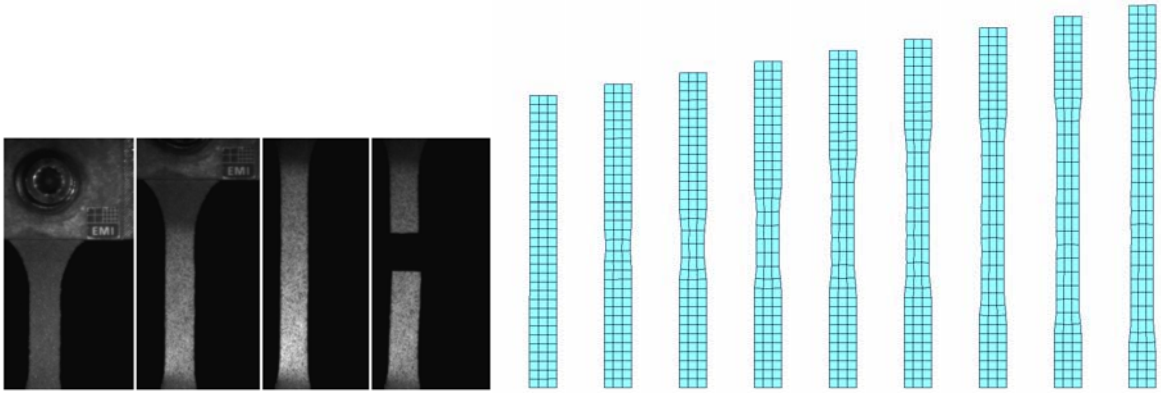

Figure 5: Tensile test and necking simulation of PP-EPDM

This type of physical response can be modeled perfectly well using standard elastic-plastic material laws although the plastic deformation of thermoplastics is not isochoric. In Figure 5, the temporal evolution of the necking simulation is shown.
A further effect which has to be considered, e.g. for leg impact simulation, is the unloading behavior of the material. This behavior can be approximated linearly by a simple damage model decreasing Young's modulus E by $E_{eff} = E(1-d)$ where $d = \hat{d}(\varepsilon_{pl})$ is a damage parameter which increases for increasing plastic strains. Usually, the damage parameter can be tabulated directly as a function of the plastic strains. In Figure 6, it is shown how the damage curve can be approximated.
It is important to know that the damage parameter also "softens" the stresses. Therefore, the stress-strain curve has to be modified in that way that the softened stresses correspond to the experimental one:

$$\sigma_{LS-DYNA} = \frac{\sigma_y}{(1-d)}. \qquad (9)$$

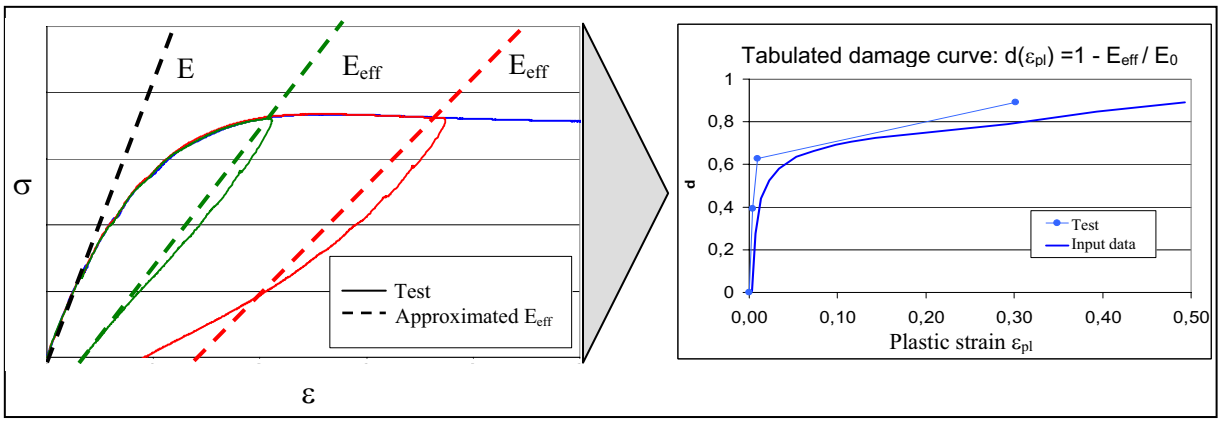

Figure 6: Modeling strategy for using damage model

The simulation results of a simple tensile test in comparison with experimental results are depicted in Figure 7. As can be seen, the reduction of the elasticity for increasing plastic strains considers approximately the unloading behavior and the experimental stress-strain curve is recovered.

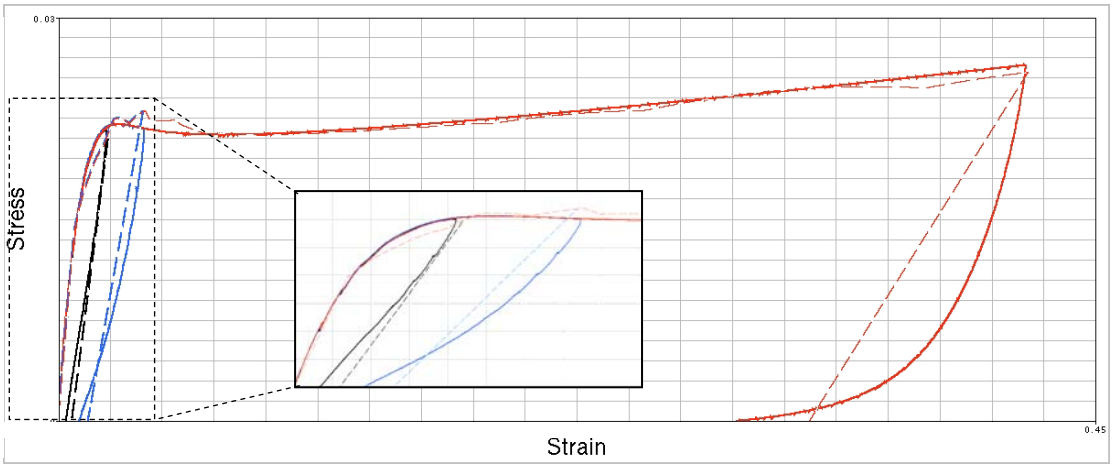

Figure 7: Simulation of the unloading behavior via damage

Finally, we consider the different behavior of thermoplastics under compression and tension, see [11] for an overview of different polymers. We use a Drucker-Prager model, see [12], [13] which is usually implemented in commercial solvers.

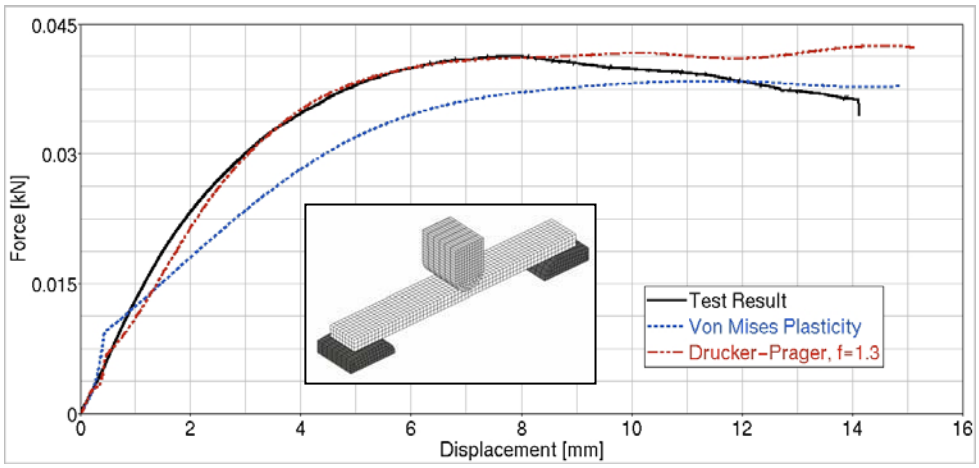

Figure 8: Three-point-bending test

In Figure 8, the reaction force versus the displacement of a quasi-static three point bending test is shown. Because of the higher yield stress under compression, it is not possible to simulate the bending test by using von Mises plasticity based on the tensile test. If a Drucker-Prager model is used where, taken from the experiment, the yield stress under compression is 1.3 times the yield stress under tension, the bending test can be simulated in a good agreement.
To sum up, it can be said that all the effects associated with thermoplastics can be approximately considered in simple material models: necking by an elastic-plastic law, unloading behavior by a damage model, differerent behavior under compression and tension e.g. by a Drucker-Prager model. However, a material model which covers all these effects is not available in commercial crash codes and has to be realized in near future.

6 Application: Pedestrian Protection

6.1 6.1 Head Impact

A typical load case regulated by laws and international standards concerning pedestrian protection is the impact of a head impactor with the engine hood. Starting with the geometrical information of the pedestrian impactor types, the Finite Element models has to be generated.
Appropriate material laws were selected to model the constitutive behavior of the skin and foam materials. In order to characterize the specific material constants, quasi static and dynamic specimen tests have been performed. Then, a validation procedure has been set up consisting of configurations which represent typical behavior of vehicle front structures. Additional experiences from applications with real car models were used to improve the FE-impactors. All headform impactors are aluminum spheres covered by thick vinyl skins. The adult (4.8 kg) and the small adult headform impactor (3.5 kg) have an outer diameter of 165 mm, the diameter of the child headform (2.5 kg) is 130 mm.

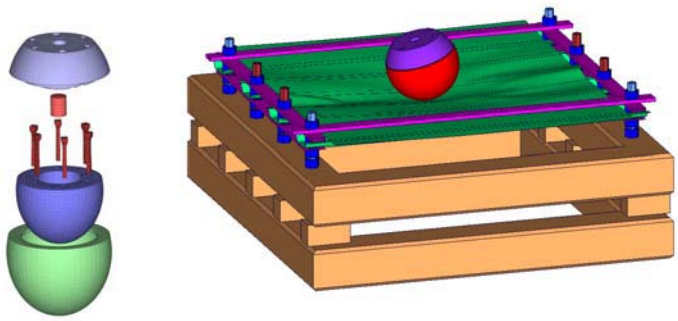

Figure 9: Headform impactors and “box” test configuration

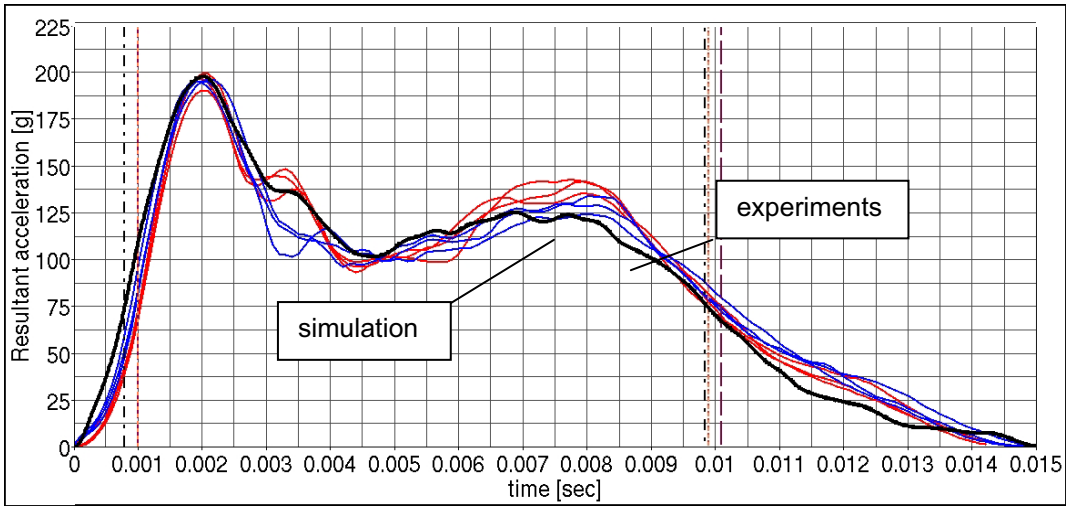

Figure 10: “Box” configuration: correlation of experiment and computation

A specific test configuration was developed with the aim to represent the behavior of a typical bonnet structure. This so called “box” configuration, see Figure 9, enables an extended validation of the head impactors under realistic conditions. The “box” test guarantees high repeatability in the experiment and is not complicated to describe in a FE-model. In Figure 10, the correlation of experiment and computation is shown. As for the vinyl skin, MAT_SIMPLIFIED_RUBBER has been used.

6.2 Leg Impact

The legform impactor consists of two metal tubes with an outer diameter of 70mm representing tibia and femur. Physical properties like mass, moments of inertia and center of gravity are specified in the EEVC-WG17 report for both femur and tibia. A layer of Confor foam (CF-45 1; thickness 25mm) is used to model the flesh. The impactor is covered by a 6 mm thick neoprene skin. For extended validation a specific test configuration was designed, see Figure 11.

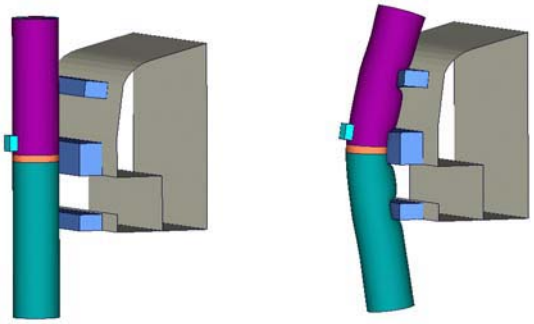

Figure 11: Leg impact test configuration for validation

This target has a wooden solid block with three pieces of foam material attached to it. Position, depth and stiffness of the foam blocks are variable. These parameters were adjusted to meet a reasonable range for all recorded signals (bending angle, tibia acceleration and shear displacement).

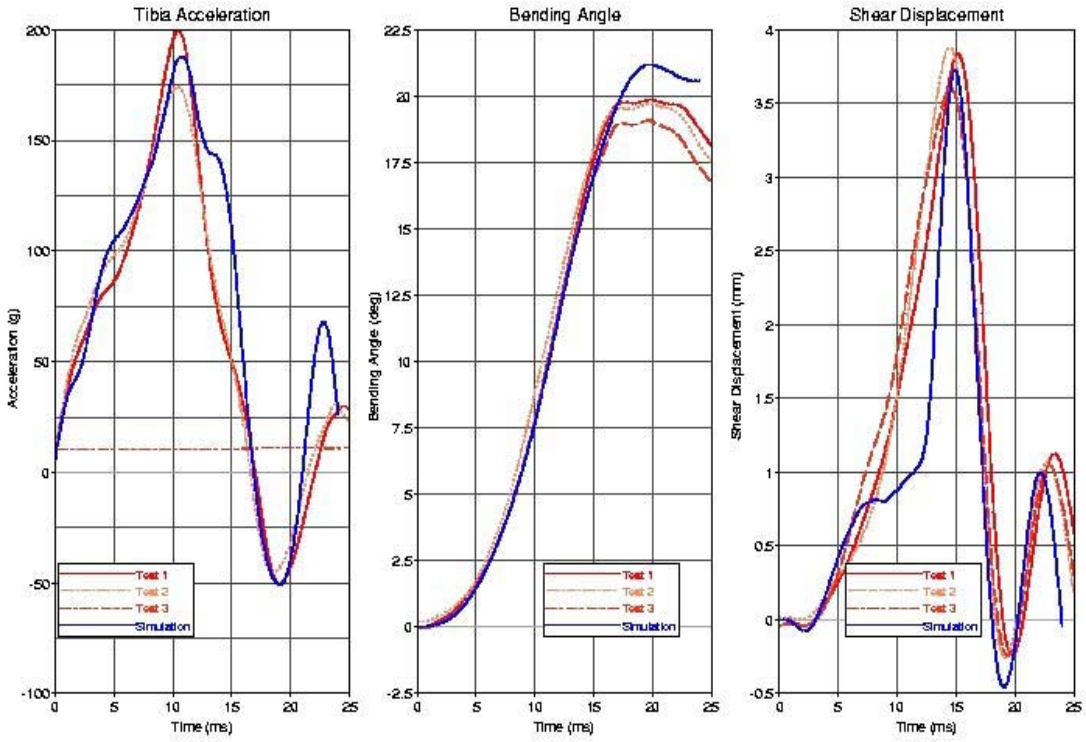

Figure 12: Validation of the leg impactor test

Calibration of the foam material has been done by performing pre-tests with a steel cylinder hitting the foam. In the validation test procedure several configurations have been analyzed: tests at different speed (40, 35 kph), variation of vertical position of the legform impactor relative to the target and angular tests (up to 15°).
A typical result of the validation procedure is shown in
Figure 12. The main focus is an overall satisfying correlation of test and simulation.

7 Conclusions

In this paper, the state-of-the-art modeling of polymeric materials in crash simulation has been shown. As for elastomers and foams, a large number of suitable material laws are available in commercial finite element programs considering incompressibility and strain rate dependency. A satisfactory situation has also been achieved with respect to user-friendliness: in particular material laws are available that allow direct input of stress-strain curves obtained from uniaxial material testing.
Thermoplastics are currently simulated using material laws based on von Mises plasticity. This approach leaves a lot to be desired. In particular, it is well known that the yield of thermoplastics in tension, compression and shear will not fit a von Mises type yield surface and that the hardening of the material is anisotropic due to reorientation of polymer chains. Furthermore, an alternative flow rule (e.g. Drucker-Prager yield surface) and, additionally, the consideration of viscosity under the yield surface are additionally desirable. Moreover, the consideration of process chain and the proper prediction of failure (damage and crack propagation), as well as the consideration of fiber reinforcements are other aspects that will have to be investigated in the future.

8 References:

[1] J.O. Hallquist: LS-DYNA, Theoretical Manual, Livermore Software Technology Corporation, Report 1018, 1991.
[2] P.A. Du Bois: Crashworthiness Engineering Course Notes, Livermore Software Technology Corporation, 2004.
[3] P.J. Blatz & W.L. Ko: Application of finite elastic theory to the deformation of rubbery materials. Trans. Soc. Rheol., 6: 223-251, 1962.
[4] M. Mooney: A theory of large elastic deformations. J. Appl. Physics, 11:582-592, 1940.
[5] R.S. Rivlin: Large elastic deformations of isotropic materials. Proc. Roy. Soc. London, 241: 379-397, 1948.
[6] R.W. Ogden: Large deformation isotropic elasticity: on the correlation of theory and experiment for incompressible rubberlike solids. Proc. Roy. Soc. London, 326: 565-584, 1972.
[7] P.A. Du Bois: A simplified approach for the simulation of rubber-like materials under dynamic loading. 4th European LS-DYNA Users Conference, pp. D-I-31/46, 2003.
[8] P.A. Du Bois, S. Kolling & W. Fassnacht: Modelling of safety glass for crash simulation. Computational Material Science, 28/3-4: 675-683, 2003.
[9] P.A. Du Bois, W. Fassnacht & S. Kolling: General aspects of material models in LS-DYNA. LS-DYNA Forum, Bad Mergentheim, Germany 2002, V2:1-55.
[10] T. Frank, A. Kurz, M. Pitzer & M. Söllner: Development and validation of numerical pedestrian impactor models. 4th European LS-DYNA Users Conference, pp. C-II-01/18, 2003.
[11] R. Bardenheier: Mechanisches Versagen von Polymerwerkstoffen. Hanser-Verlag, 1982.
[12] D.C. Drucker, W. Prager: Soil mechanics and plastic analysis or limit design. Quaterly of Applied Mathematics, 10:157-165, 1952.
[13] D.C. Drucker: A definition of stable inelastic material. Journal of Applied Mechanics, 26:101-106, 1959.
[14] R. Hill: Aspects of invariance in solid mechanics. *Adv. Appl. Mech.* 18: 1–75, 1978.
[15] B. Storåkers: On material representation and constitutive branching in finite compressible elasticity. J. Mech. Phys. Solids, 34(2): 125-145, 1986.
[16] P.A. Du Bois, S. Kolling, M. Koesters & T. Frank: Material modeling of polymeric materials in crashworthiness analysis. 3rd Workshop for Material and Structural Behaviour at Crash Processes (*crash*MAT), Freiburg, Germany 2004.
[17] P. A. Du Bois, S. Kolling & T. Frank: Material behaviour of polymers under impact loading. International Symposium on crashworthiness of light-weight automotive structures, Trondheim, Norway, 2004.

